

Document downloaded from:

<http://hdl.handle.net/10251/165615>

This paper must be cited as:

Pallarés Rubio, L.; Pallarés Rubio, F.J.; Ramada, JR.; Agüero Ramón Llin, A.; Eatherton, MR. (2020). Monotonic shear strength of headed studs in reinforced infill walls. *Engineering Structures*. 205:1-18. <https://doi.org/10.1016/j.engstruct.2019.110045>



The final publication is available at

<https://doi.org/10.1016/j.engstruct.2019.110045>

Copyright Elsevier

Additional Information

MONOTONIC SHEAR STRENGTH OF HEADED STUDS IN REINFORCED INFILL WALLS

L. Pallarés*, José R. Ramada*, Francisco J. Pallarés*, Antonio Agüero*, Matthew R. Eatherton**

*Universitat Politècnica de València, Camino de Vera, s/n. 46022. Valencia. Spain

**Virginia Tech. Dept. of Civil and Environmental Engineering, 105D Patton Hall, Blacksburg, VA 24060.

SUMMARY

Headed studs are key components of structures which facilitate composite behavior between steel and concrete elements. In steel building structures, reinforced concrete infill walls surrounded by a stiff steel frame is a common example of a composite structure used to resist horizontal loads such as those produced by earthquakes or wind. To this end, these types of concrete walls need to be anchored to the steel frame with headed studs which must withstand shear and tensile forces (AISC 360). To properly design headed stud anchors in concrete walls, it is first necessary to understand their behavior when subjected to monotonic shear forces considering edge conditions and reinforcing details that may influence the stud strength.

Few tests have examined headed studs subjected to monotonic shear with typical boundary effects in reinforced infill walls, so a new experimental study on 17 specimens explores the behavior of headed studs exposed to monotonic shear loading with group effects. The experiments showed that the strength of studs installed in infill walls with edge conditions is well predicted (average error in prediction is smaller than 10%) by ACI 318, AISC 360 and EC-4. However, when group effects of anchors are included in the analysis of infill walls, only the ACI 318 is able to predict the behavior.

1. INTRODUCTION

Headed studs are widely used to facilitate composite behavior between steel and concrete elements. For instance, studs are placed in composite beams, columns and walls to obtain benefits of both the steel and concrete.

In steel building structures, composite beams are common, and usually consist of a concrete slab connected to a steel beam with headed studs. More examples of composite behavior in structures are composite columns and steel frames with reinforced concrete infill walls (herein SFRCIW, see *Figure 1*), attached to a steel frame around the perimeter of each wall panel. Currently, infill concrete walls are designed to stiffen steel frames to resist horizontal loads from earthquakes or wind, and they act as the primary lateral force resistance system for some steel-framed buildings (Morelli et al. 2019). These types of infill concrete walls need to be anchored to the surrounding steel frame with headed stud anchors subjected to shear and tensile forces. For the studs, the slenderness ratio of the anchors (h_{ef}/ϕ) is a fundamental parameter that differentiates the type of failure mode as either an undesirable brittle failure of the concrete or a ductile failure in the steel.

To properly design headed stud anchors in SFRCIW, it is necessary to understand their behavior under monotonic shear loading with boundary conditions typical of reinforced infill walls. Studies

related to headed studs subjected to monotonic forces are numerous; however, there is little research related to headed studs subjected to shear or tension with boundary conditions similar to those in infill walls (Pallarés and Hajjar 2010).

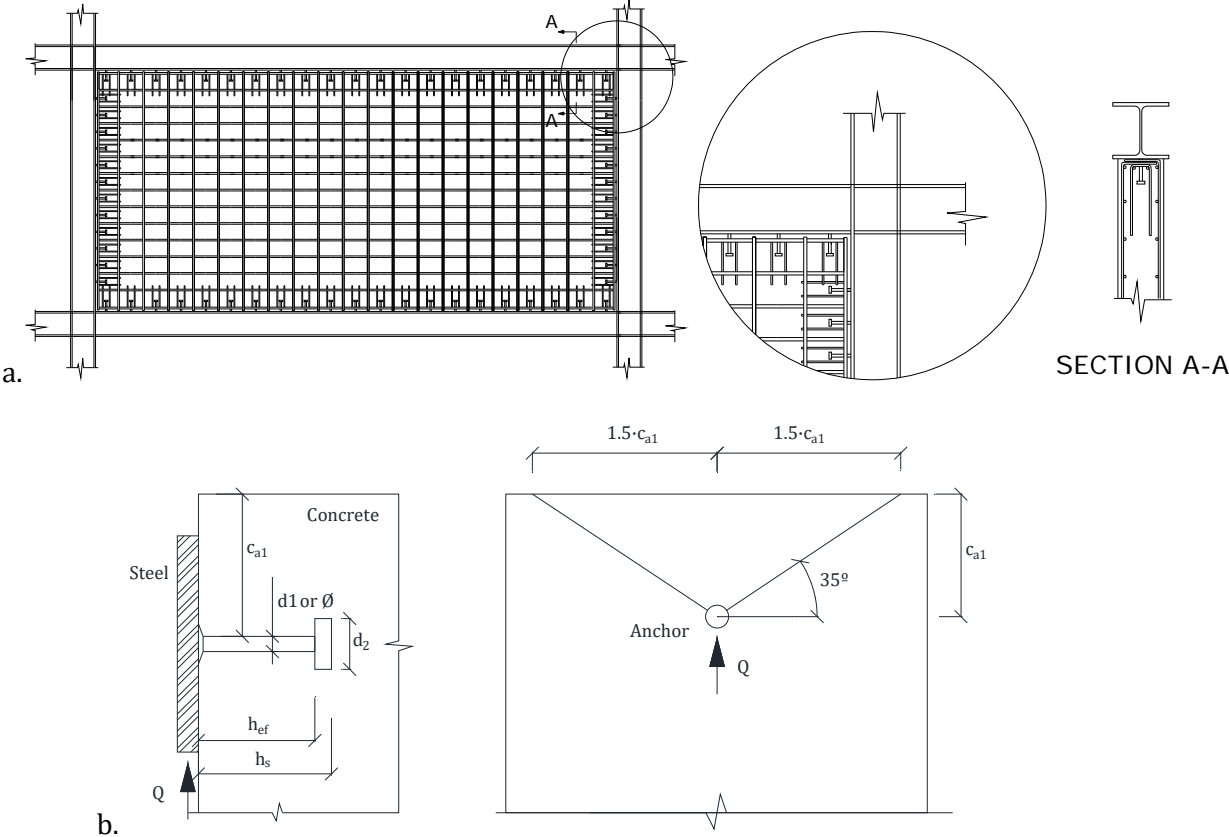


Figure 1. a) Detail of a stud and reinforcement in a composite wall (AISC 360). b) Geometric dimensions of a headed stud and concrete breakout definition.

The headed anchors described in AISC 360 (AISC 2016) are steel anchors that fulfill requirements established in AWS D1.1 (2004); these are anchored to a steel plate before pouring the concrete. Geometric dimensions of the headed studs are described in Figure 1.b. These studs are described by their primary dimensions, diameter of the shank (ϕ or d_1) and the height (h_s). Another relevant dimension is h_{ef} or effective height, i.e. the embedded length from the underside of the head to the concrete surface.

Pallarés and Hajjar (2010) carried out an extensive literature review including 391 tests on headed studs subjected to monotonic shear in order to analyze types of failure, evaluate formulas for design strength of anchors, and propose a strength formula based on the 391 tests. It is noted, however, that there are very few tests involving cyclic shear loading.

During an earthquake, anchors can be exposed to tensile force, shear force, or a combination of the two, and many variables such as cracks in concrete or changing force directions may influence the behavior of a headed stud. Research by Hawkins and Mitchell (1984), Gattesco and Giuriani (1996), Bursi and Ballerini (1996), Zandonini and Bursi (2002), and Civjan and Singh (2003) describe a range of push-pull tests on shear connectors under high amplitude cyclic (seismic) shear loading for slabs in composite beams without edge conditions.

The majority of the research into the behavior of steel frames with reinforced concrete infill walls has been done in Japan, e.g. Makino (1985) and recently in Italy (Morelli et al. 2018, Dall’Asta et al. 2017) and has focused on transferring the struts formed in the concrete between the joints of the steel frame. Makino (1985) performed experiments on single story, single bay SFRCIW at approximately a one-third scale. Makino (1985) recommended a formula for stud strength as

$$Q = \phi \cdot (0.5 \cdot A_s \sqrt{f_c \cdot E_c}) \quad (1)$$

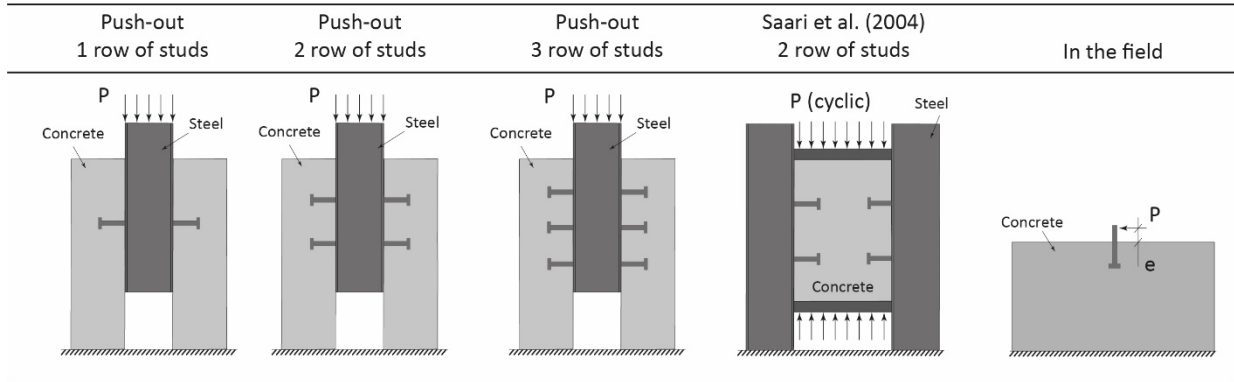
Where $\phi = 0.6\phi_1$ is an edge reduction factor, $\phi_1 = \sqrt{a/15}$, a is the distance from the center of the stud to the edge of the panel in cm, A_s is the cross-sectional area of the shear stud in cm^2 , f_c is the concrete compressive strength in kg/cm^2 and E_c is the modulus of concrete in kg/cm^2 . This formula is similar to the strength formula in the AISC Specification (AISC 360) in cases when concrete failure governs, with an additional term, ϕ_1 , intended to reduce the stud capacity in the case of thin walls.

However, the testing configuration is relevant to determine the strength of the headed studs. The push-out test (*Figure 2*), a variant of push-out or “in the field” are the most common test configurations used to study shear connectors. Push-out tests might not represent pure shear tests since tension is introduced together with shear when steel anchors are loaded because of the eccentricity of the load (Civjan and Singh 2003, *Figure 2*). Furthermore, the push-out test configuration does not allow for testing with edge conditions or controlled interaction of shear and tensile forces. Finally, conventional push-out tests cannot simulate the cyclic load behavior of studs during an earthquake.

This paper describes a new test setup which subjects headed studs to special edge conditions typical of infill walls with several advantages:

- The proposed test setup allows shear and tensile loads to be applied to the headed studs as seen in the case of those installed in the SFRCIW (*Figure 1*).
- The proposed test simulates the edge conditions of the SFRCIW, that is, bearing against concrete that has a free edge in the direction of the load and free lateral sides. These free edges must be reinforced with steel hairpins to prevent the breakout failure. To this end, the proposed test allows local failure of the concrete around the headed studs (pryout failures) and failures in the steel. Likewise, the tests simulate the influence of the wall reinforcement on the behavior of the headed studs.
- The proposed test setup allows the load to be introduced with the minimum possible eccentricity between the applied load and the steel-concrete interface. Thus, the appearance of undesirable tensile forces in the headed studs is avoided.
- The proposed test setup allows for both cyclic shear and tensile loads to be applied, as the case in those installed in the SFRCIW (*Figure 1*).

TYPES OF CONFIGURATION



SCHEMATIC STATE OF STRESS

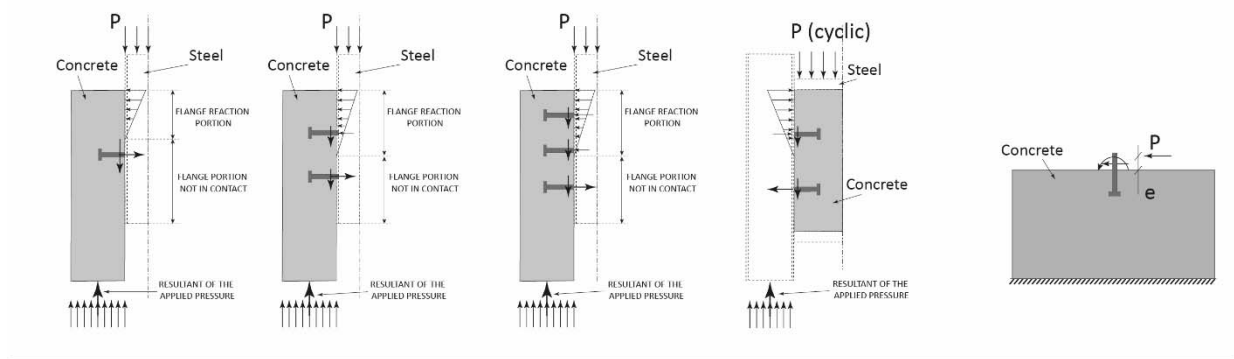


Figure 2. Test Layout for shear loading of headed studs (Pallarés and Hajjar 2010) and schematic state of stress.

2. RESEARCH SIGNIFICANCE

Given the scarcity of research into headed studs subjected to cyclic shear, a new experimental program including 17 specimens is presented in this paper. The program examines the behavior of headed studs under shear loading and group effects with edge conditions typical of infill walls. This new test setup eliminates some of the disadvantages of push-out tests. The proposed test procedure aims to determine how edge conditions and group effects influence the strength of the head studs installed in the SFRCIW as well as, which reinforcing details prevent breakout failure.

3. EXPERIMENTAL PROGRAM

The majority of headed stud anchors tested in this research have sufficient embedded length ($h_{ef}/\phi > 4,5$) to reach a ductile failure in the steel when subjected to shear force, avoiding brittle failures in the concrete such as pryout failure as defined in ACI 318 (2008). Furthermore, reinforcing steel is incorporated into the concrete block to prevent concrete breakout failures in accordance with ACI 318, similar to the reinforcing in a RC infill wall.

The steel reaction frame and test setup, as well as the variables considered in the design of the experimental program, are described in the following section.

3.1. TEST SETUP

A new self-reacting steel reaction frame was designed to test headed studs welded to a piece of steel beam (IPE 200 in *Figure 3*) and embedded in a rectangular prismatic reinforced concrete specimen. This specimen was intended to represent the local behavior, at full scale, of the shear stud connection in SFRCIW.

A hydraulic actuator with a 1000kN capacity (*A* in *Figure 3*) was horizontally oriented in the steel frame and equipped with a HBM U10 tensile-compression load cell with 500kN range (*B* in *Figure 3*). Next to the load cell, a large pin connection, which was free to rotate in the plane of the specimen, was bolted to the testing machine. The pin was connected to a collar that enveloped the steel beam at both ends (*C* in *Figure 3*). To accommodate fully reversed shear loading, a threaded rod system was utilized. Two steel blocks (*D* in *Figure 3*) were located between the steel beam and collar. Since the line of action of the actuator load was 1mm above the steel and concrete interface (*E* in *Figure 3*), shear force dominated over tension in the headed studs. This configuration also allowed for future testing of anchors under combined tension and shear forces when an actuator is added between the steel beam and the upper beam of the steel reaction frame. A picture of the steel reaction frame is shown in *Figure 4*.

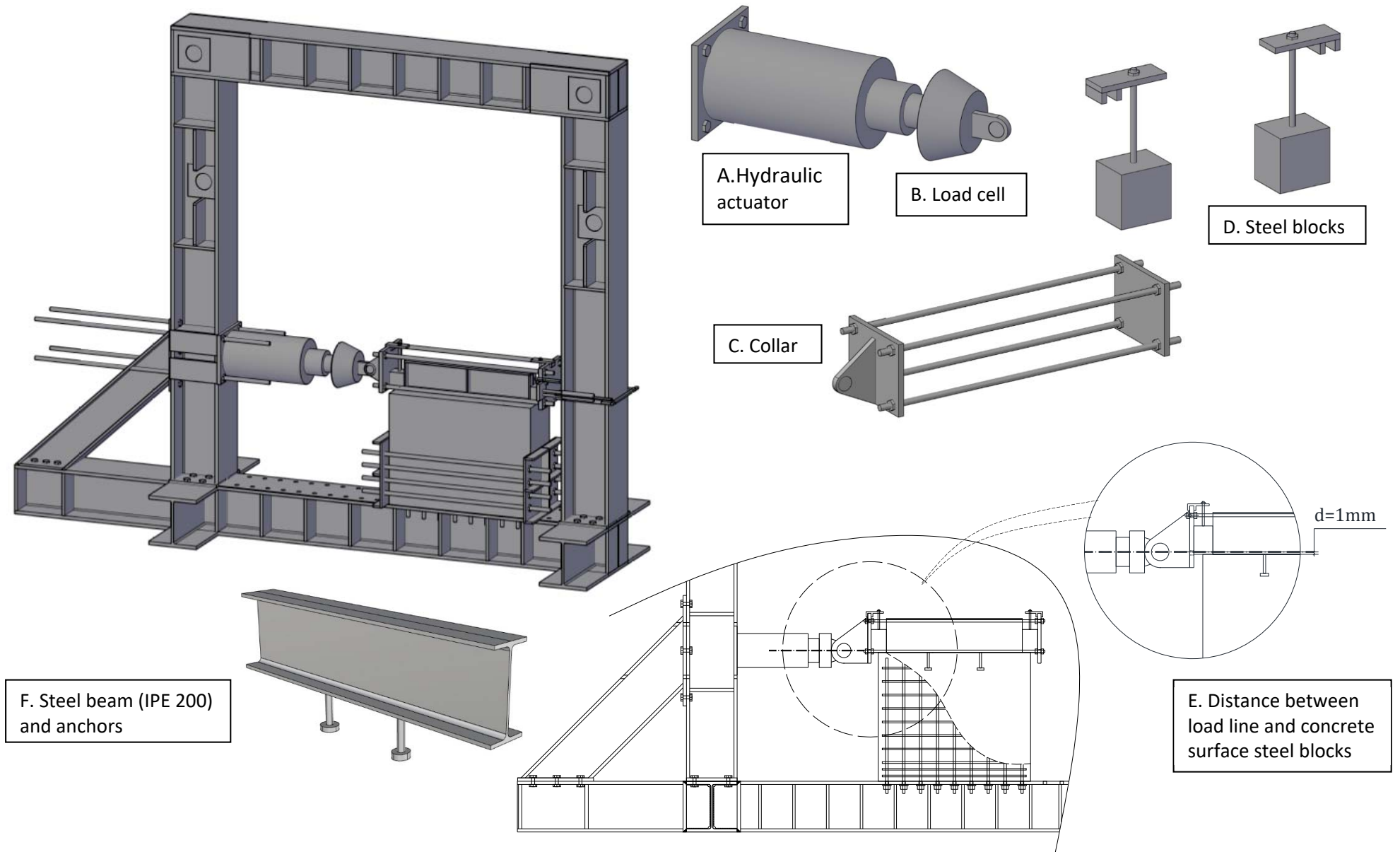


Figure 3. Test layout for shear force.



Figure 4. Test setup for headed studs in reinforced concrete panels subjected to shear forces.

3.2. SPECIMENS AND VARIABLES

The specimen is formed by a piece of steel beam IPE200 that is 820mm in length, where headed studs are welded according to the desired specimen configuration (*Figure 5.a*). Once the studs are welded, they are inserted in the steel reinforcing cage and molds (*Figure 5.b*, *Figure 5.c*) and then the concrete is poured (*Figure 5.d*).

The concrete part of the specimen (*Figure 6*) is 745mm tall and 300x900mm (dimensions from a top view). This concrete block may simulate the upper portion of a concrete infill wall with embedded steel anchors and a high density of stirrups to control breakout failure.

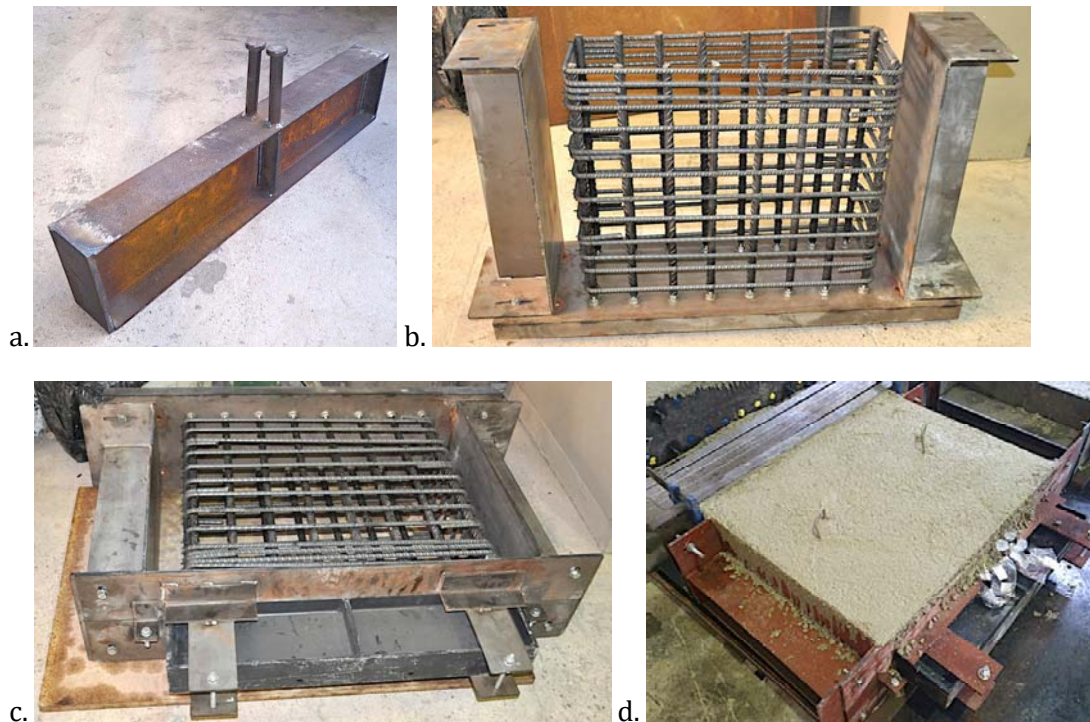


Figure 5. Specimen production. a) steel beam with welded headed stud anchors, b) reinforcement of the specimens and steel form, c) steel beam with headed stud anchors and steel cage before pouring the concrete. d) specimen after pouring the concrete.

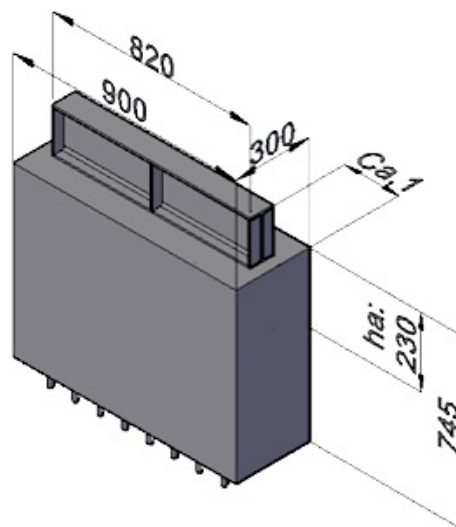


Figure 6. Specimen to be tested (in mm).

The variables examined in this study are: diameter (ϕ), height (h_{ef}) of headed studs and ratios of effective height over diameter (h_{ef}/ϕ from 4.19 to 7.37).

According to the number of studs and distances between them, four configurations are investigated:

- *Single Stud (SS)*. A single stud is located in the center of the steel beam (Figure 7.a).
- *Single row of studs without group effects (SRS)*. The distance between studs in the load direction is defined as m , and a sufficient distance is used to discourage group effects

between studs (*Figure 7.b*). In order to minimize group effects related to pryout failure according to ACI 318, the studs are separated at least $3h_{ef}$.

- *Two Rows of Studs with Group Effects (TRS-GE)*. Two studs are welded to the steel beam with a spacing that is orthogonal to the load direction. The distance between studs is defined as s . This configuration is a common design in engineering practice and is considered to assess group effects under cyclic load conditions (*Figure 7.c*). The distance, s , is varied from $[0.32 h_{ef}$ to $0.55 h_{ef}]$.
- *Single Row of Studs with Group Effects (SRS-GE)*. In this case, two studs are welded to the steel beam with a spacing in the load direction. The distance between studs in the load direction, t , takes into account interactions between studs due to group effects (*Figure 7.d*). The distance, t , is varied from $[0.47 h_{ef}$ to $0.52 h_{ef}]$.

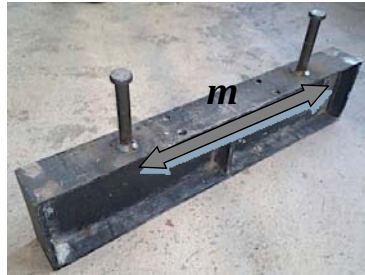
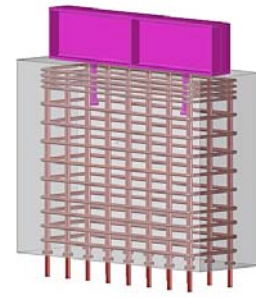
The testing program was designed to vary the stud diameter, height, configuration, and stud spacing as described in the preceding paragraphs. Typical stud diameters in the design of SFRCIW were chosen (16mm, 19mm and 22mm). A range of slenderness of the studs was tested with a minimum of 4.5 up to a maximum of 7.37 to explore the effect of slenderness and edge conditions on the capacity of the studs. *Table 1* shows the resulting specimens and the dimensions, m , s , and t , which define the locations of studs on the steel beam.

Table 1. Specimens.

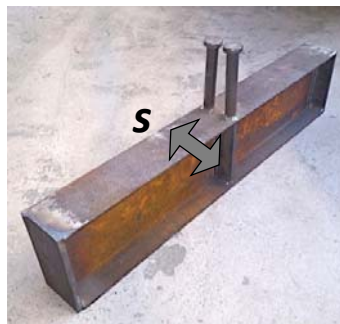
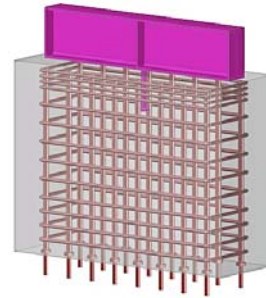
Stud Configuration	#Specimen	Φ (mm)	h_{ef} (mm)	Number of Headed Studs	h_{ef}/Φ	$m/s/t$ (mm)	f_c (MPa)
SS	18	19	100	1	4.74	-	24.5
SS	19	19	100	1	4.74	-	41.4
SS	21	19	150	1	7.37	-	41
SS	23	22	150	1	6.36	-	37.5
SRS	2	16	75	2	4.19	225	48.4
SRS	5	19	100	2	4.74	300	24.5
SRS	6	19	100	2	4.74	300	41.4
SRS	11	19	150	2	7.37	450	41.4
SRS	14	22	150	2	6.36	450	48.4
SRS	15	22	150	2	6.36	450	41.4
TRS-GE	26	19	100	2	4.74	49.5	24.5
TRS-GE	27	19	100	2	4.74	42	41.4
TRS-GE	29	19	150	2	7.37	59	41.4
TRS-GE	31	22	150	2	6.36	44	41
SRS-GE	33	19	100	2	4.74	44	37.5
SRS-GE	35	19	150	2	7.37	64	41.4
SRS-GE	37	22	150	2	6.36	65	37.5



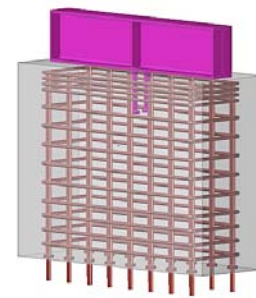
a. SS configuration



b. SRS configuration



c. TRS-GE configuration



d. SRS-GE configuration

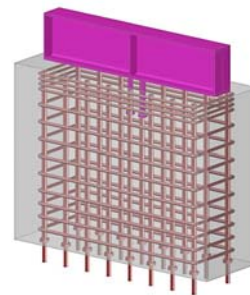


Figure 7. Studs configuration.

3.3. MATERIALS

The specimens were designed with concrete and steel:

a. Concrete: Two cylinder specimens (height of 300mm and diameter of 150mm) were cast and tested to determine the concrete strength at the time of the headed stud test. Concrete strength varied from 25 to 40MPa and is provided for each specimen in the *Tables 3, 4, 5 and 6.*

b. Steel of headed studs: the properties of the steel provided by the manufacturer are shown in *Table 2* such as: type of steel, ultimate stress of the steel (f_u), yield stress of the steel (f_y), minimum strain at ultimate stress (A_5), composition and resistance features.

Table 2. Steel properties of headed studs.

Steel Material	f_u (N/mm^2)	f_y (N/mm^2)	A_5	Composition	Strength properties
St-37.3K	450	350	15%	DIN-17.100	DIN 50.049
S235J2G3+C450	450	450	15%	ETA-03/0039	EN 10025:2005

3.4. TEST PROCEDURE AND INSTRUMENTATION

The tests were conducted using displacement control with a constant rate of 0.1 mm/s applied monotonically up to failure. Load was measured using the load cell located between the actuator and specimen as described previously. An LVDT was located on the side of the specimen opposite the actuator to measure the slip between steel and concrete.

Completing the instrumentation, strain gauges are applied at the midheight of the studs to measure axial strains along the studs (*Figure 8*). Two strain gauges are glued on each stud parallel to the stud. The gauges are HBM type LY41 strain gauges with 3mm grid length and 120 Ohm electrical resistance. The strain gauges are placed to determine the behavior of the stud during the test and provide information about the failure mode as described in section 4.1.

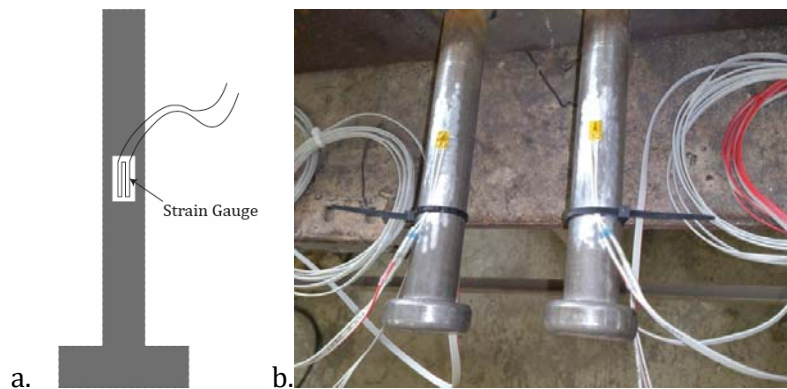


Figure 8. Strain gauges at midheight of studs. a) Scheme of strain location and direction, b) strain gauges glued to the studs.

4. EXPERIMENTAL RESULTS AND COMPARISON WITH DESIGN EQUATIONS

Experimental results are compared with the theoretical shear strength obtained from provisions of ACI 318, AISC 360, EC-4 and predictions provided by Makino (1985) for shear studs in SFRCIW. Test-to-predicted ratios (ξ) according to Eq. 2 are provided to assess the accuracy of prediction equations.

$$\xi = \frac{Q_{test}}{Q_{theoretical}} \quad (2)$$

where:

Q_{test} peak load obtained in the test

$Q_{theoretical}$ predicted load according to ACI 318-08 Appendix D in concrete pryout failure and steel failure.

ACI 318 includes a set of equations for the strength of anchors. The provisions consider many types of configurations and failure modes, but only concrete pryout failure (Q_{cp}) in the vicinity of the anchor due to shear loading and steel failure is considered for components with composite behavior. ACI 318 includes several other failure modes such as breakout or side blowout, but these are not relevant because anchor reinforcement is used in the specimens to preclude these types of failure modes. The strength associated with concrete pryout is given in ACI 318 as:

$$Q_{cp} = k_{cp} N_{cb} \quad (3)$$

where:

$k_{cp} = 2$ if $h_{ef} \geq 2.5$ in

$N_{cb} = \frac{A_{nc}}{A_{nco}} \Psi_{ec,N} \Psi_{ed,N} \Psi_{c,N} \Psi_{cp,N} N_b$ is the concrete breakout strength for a group of anchors;

$\Psi_{ec,N}$ is the modification factor for anchor groups loaded eccentrically in tension. In this case, they are loaded concentrically, so this factor is 1.

$\Psi_{ed,N} = 0.7 + 0.3 \frac{c_{a,min}}{1.5 * h_{ef}} \leq 1$ is the modification factor for edge effects.

$\Psi_{c,N} = 1.25$ for cast-in anchors is the factor to account for cracking.

$\Psi_{cp,N} = 1$ for cast-in anchors where supplementary reinforcement is provided to control splitting or in the regions with cracking in the concrete.

$N_b = k_c * \lambda * \sqrt{f_c'} * h_{ef}^{1.5}$ where $k_c = 24$ for cast-in anchors.

λ is the modification factor for lightweight concrete. It is equal to 1 in normal-weight concrete.

$A_{nc} = 3 * h_{ef} * (c_{a1} + 1.5 * h_{ef})$ (see Figure 1.b)

$A_{nco} = 9 * h_{ef}^2$

To compute the failure in the steel, ACI 318 assumes a tensile failure of the shank and proposes the following equation:

$$V_{sa} = n * A_{sa} * f_u \quad (4)$$

where

n is the number of studs,

A_{sa} is the cross-sectional area of the headed stud anchor

The design shear resistance of a welded headed stud is determined in EC-4 from:

$$Q = \frac{0.8 f_u \pi d^2 / 4}{\gamma_v} \quad (5)$$

or:

$$Q = \frac{0.29 \alpha d^2 \sqrt{f_{ck} E_{cm}}}{\gamma_v} \quad (6)$$

whichever is smaller, with

$$\alpha = 0.2 \left(\frac{h_{ef}}{\phi} + 1 \right) \text{ for } 3 \leq h_{ef}/\phi \leq 4 \quad (7)$$

$$\alpha = 1 \text{ for } h_{ef}/\phi \geq 4 \quad (8)$$

Where:

γ_v is the partial factor, taken as being equal to 1 in this verification

d is the diameter of the shank of the stud, $16\text{mm} \leq d \leq 25\text{mm}$

f_u is the specified ultimate tensile strength of the material of the stud but not greater than $500\text{N}/\text{mm}^2$

According to AISC 360, steel headed stud anchors subjected only to shear shall not be less than five stud diameters in length. When concrete breakout strength is not an applicable limit state, the design shear strength is determined as follows:

$$Q = n f_u A_{sa} \quad (9)$$

where

A_{sa} is the cross-sectional area of the headed stud anchor.

AISC 360 precludes concrete failure due to the slenderness restrictions and minimum spacing of $3h_{ef}$ between anchors to avoid group effects.

It should be noted that EC-4 and AISC 360 were not intended specifically for SFRCIW with edge conditions or group effects, but generally for composite actions in beams. In the specimens tested herein, free edges are restrained to avoid breakout by stirrups located at the top of the specimen so these formulas might be applied for design in the absence of group effects.

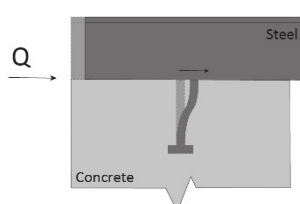
4.1. FAILURE MODES

Failure was classified into three types: failure in the steel, failure in the concrete and mixed failure of steel and concrete. The failure in the steel can be detected by visual inspection observing a shear rupture in the section of steel (Mode 1.a in *Figure 9*) or through the strain measurement of strain gauges glued to the shank of the anchor whether it is subjected to tensile forces (Mode 1.b).

FAILURE MODES IN HEADED STUD ANCHORS INSTALLED IN REINFORCED INFILL WALLS

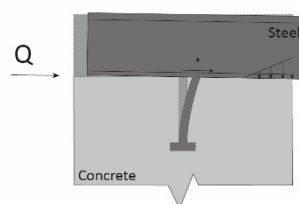
MODE 1. STEEL FAILURE

Proposed in two ways according to shear or tension stresses in the stud, respectively.



Mode 1.a. EC-4

$$Q_n = \frac{0.8 f_u A_{sa}}{\gamma_v}; \gamma_v = 1.25$$



Mode 1.b. AISC 360 / ACI 318

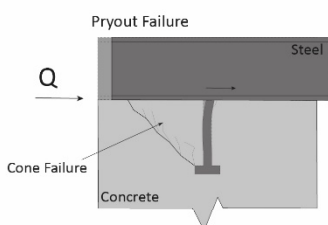
$$Q_n = \phi A_{sa} f_u; \phi = 0.65$$

Experimental Criterion: rupture in the cross section of steel.

MODE 2. CONCRETE FAILURE

Pryout failure: failure in the vicinity of the headed stud. A cone failure in concrete.

Breakout failure: a breakout prism is formed due to a free edge.

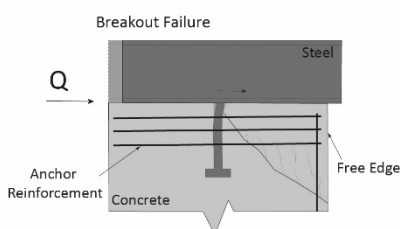


EC-4: only predicts *pryout* failure.

$$Q_n = \frac{0.29 \alpha \phi^2 \sqrt{f_c E_c}}{\gamma_v} \text{ with: } \alpha = 0.2 \left(\frac{h}{\phi} + 1 \right) \text{ for } 3 \leq h/\phi \leq 4$$

$$\alpha = 1 \text{ for } h/\phi > 4$$

AISC 360: precludes concrete failure for composite components in the vicinity of concrete (*pryout*) if $h/\phi > 5$. If *concrete breakout* strength is an applicable failure (for example, where the breakout prism is not restrained by an adjacent steel plate, flange or web), appropriate anchor reinforcement is required.



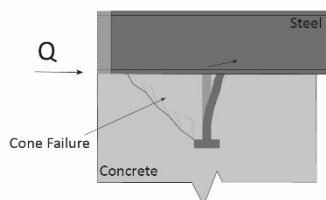
ACI 318: concrete *pryout* failure according to equation (3). *Concrete breakout* strength is restrained with appropriate anchor reinforcement.

Experimental Criterion: Small strains in the steel measured with the strain gauges and concrete failure in the vicinity of the headed studs.

MODE 3. MIXED STEEL-CONCRETE FAILURE

Failure of concrete in the vicinity of the headed stud and large tensile strains in steel.

A cone failure concrete and steel in tensile are formed.



Experimental Criterion: Large strains ($>1750 \mu\epsilon$) but not steel failure (rupture in cross section) and concrete failure in the vicinity of the headed studs.

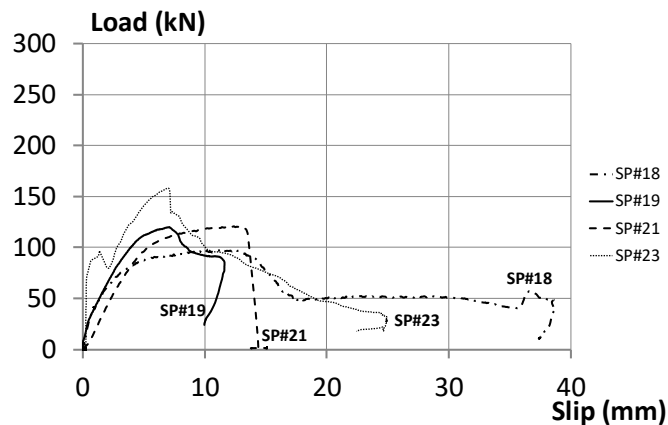
Figure 9. Failure modes of headed stud anchors in SFRCIW.

The first failure mode in the steel, described as a steel shear failure (Mode 1.a), may be estimated by EC-4 (2004), $0.8 f_u A_{sa}$ through the reduction coefficient 0.8 applied to the full capacity of the steel in tension, while the second failure concept (Mode 1.b) in the steel subjected to tensile forces is proposed by AISC 360 and ACI 318 ($f_u A_{sa}$). The experimental criterion consists of reaching a

rupture in the steel section of the stud. By contrast, concrete failure in the specimen occurs when the strains in the steel are small, and failure occurs due to the formation of the concrete cone failure as proposed by ACI 318 in accordance with pryout failure. In composite members, concrete breakout strength is an applicable concrete failure according to AISC 360, which may be restrained with an appropriate anchor reinforcement. Mixed failures of both steel and concrete can result in both concrete cone failure and steel strains close to the yield point. An experimental criterion for mixed failures is based on undergoing large strains ($>1750\mu\epsilon$) in the shank of the stud and considerable degradation of concrete is observed without reaching a cross section rupture in the shank.

4.2. SINGLE STUD CONFIGURATION (SS)

The load-slip curves of Specimens #18, #19, #21 and #23 are plotted in *Figure 10*. Values of experimental results in the SS configuration are shown in *Table 3*,



Specimen #18($h_{ef}/\phi=4.6$; $\phi=19\text{mm}$); Specimen #19($h_{ef}/\phi=4.6$; $\phi=19\text{mm}$); Specimen #23
($h_{ef}/\phi=6.14$; $\phi=22\text{mm}$); Specimen #21($h_{ef}/\phi=7.37$; $\phi=19\text{mm}$)

Figure 10. Load-slip curves for SS configuration.

Specimens #18 and #19 used the same geometry with the only difference being the concrete strength. Specimen #19 had a concrete strength of 41.4MPa while that of Specimen #18 was 24.5MPa. The peak load of Specimen #19 (120.3kN) was 23% larger than Specimen #18 (97.7kN). Both specimens showed mixed failure of steel and concrete, with concrete strength proving to be a variable influencing the peak load. *Figure 12* shows substantial concrete failure in Specimens #18 and #19, but these are considered mixed failure because strains in the steel shank exceeded yield strains (0.00175 m/m see *Figure 13*), and the concrete in the vicinity of the stud was highly degraded. In load-strain curves (*Figure 13* and *16*), it can be observed that studs with greater slenderness were better anchored in the concrete (Specimen #21 and #23), and presented lower strain as registered by the gauges located along the axis. In these cases, the stud was basically subjected to shear forces (*Figure 9.a*) instead of tensile ones. In these cases, when the strains suddenly increased it meant that the concrete located in the vicinity of the stud (at the top) cracked and the stud was subjected to tensile forces.

Nevertheless, high strength concrete (around 40MPa) allowed the specimens to reach loads close to the steel strength, so h_{ef} / ϕ of 4.63 is considered the slenderness that allows for development of the stud strength in high strength concrete. In this sense, Specimen #21 shows a clear example of a failure in the steel for concrete strength of 41MPa implying that it had more than sufficient development length to reach the stud shear strength.

Failure surfaces of the concrete exhibited the expected pyramid shape (Specimens #18 and #19 in *Figure 12*) according to the Concrete Capacity Design (CCD) approach described in ACI 318 (see Mode 2 in *Figure 9*).

One may observe how this pyramid reached the lateral free edges. Breakout concrete failure, that is a failure in the front edge of the wall, was precluded due to the stirrups on the upper side of the specimen. Specimens #18 and #19 (*Figure 12*) did not reach the estimated pryout load (104.75kN and 133.37kN, respectively in *Table 3*), but the steel reached the yield strain. Specimen #18 exhibited a stud strain that exceeded the yield strain (0.00175 m/m) and generated a breakage of concrete in its vicinity. By contrast, specimen #19 presented a failure in the concrete with a curve similar to that of Specimen #18, but with a larger load obtained.



Figure 11. Steel failure in Specimen #21.

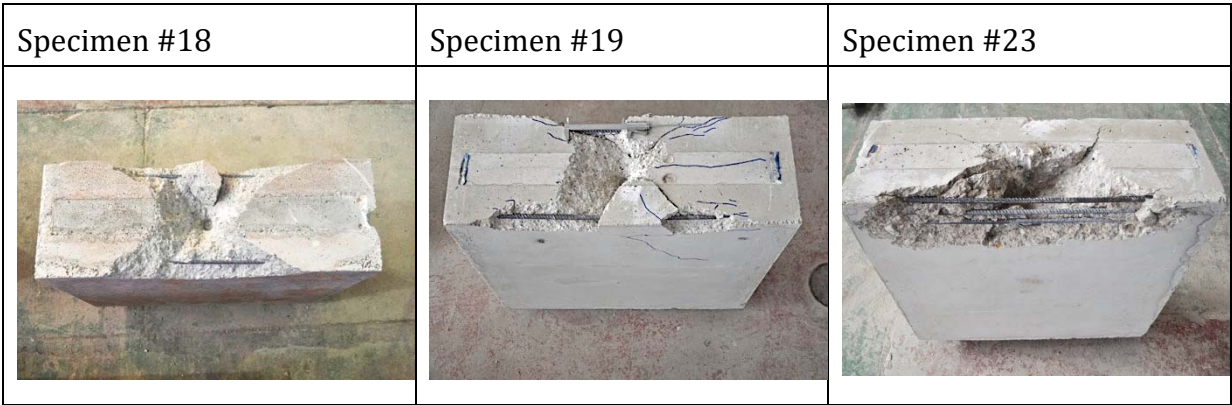
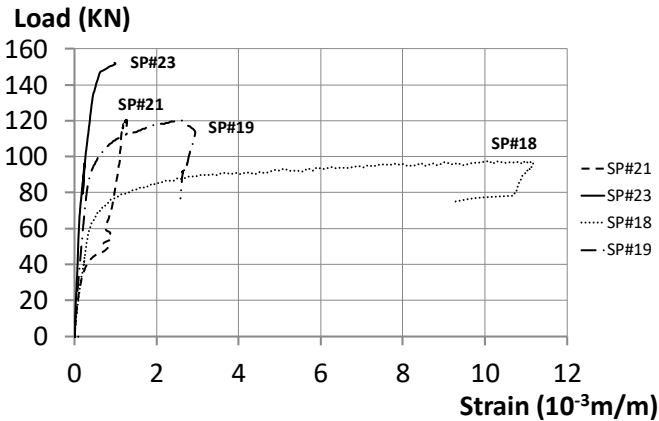


Figure 12. Mixed failures in concrete and steel for SS configuration.

Specimen #21 showed a clear failure in the steel stud in one plane perpendicular to the stud axis and above the collar weld (*Figure 11*). This specimen with a development length in the concrete of 7.37 (h_{ef} / ϕ), was well anchored and produced a failure in the steel stud with strains in the direction of the shank around 0.001 m/m. Therefore, this type of failure with clearly shank in shear (see

Figure 11) could not be predicted by the tensile strength formula. Specimen #23 presented a lateral concrete failure formed on one side of the pyramid (Figure 12) and cracks started to form on the other side when concrete pryout occurred in the test, being well predicted by concrete failure estimation of ACI 318 (test-to-predicted is 0.958 in Table 3).

The average peak load from the experimental tests was $0.894 A_s f_u$ (Table 3), which is 11% smaller than the steel failure strength predicted by ACI 318 or AISC 360. Some of this difference may be because the average was calculated including tests in which the stud failed and those presenting mixed failure of concrete and steel. This reduction might also be because the shank is subjected locally to a combination of shear, flexure and tensile forces, not just shear. It was shown in past testing that the stud is able to resist a shear force close to $f_u A_{sa}$, instead of the value $f_u A_{sa} / \sqrt{3}$ that would be expected for shear, because the welded collar creates a larger section at the base and transfers part of the shear force (Pavlovic et al. 2013). The prediction by EC-4 ($0.8 A_s f_u$) is shown to be more accurate relative to the current data set in terms of steel failure strength. When the rest of the provisions in EC-4 are included, the prediction becomes conservative as shown by the minimum of the concrete and steel strength prediction. The prediction of EC-4 averages 1.217 times the experimental strength as given in Table 3. ACI 318 is the most accurate of the three provisions for which the minimum calculated concrete and steel strength results in an average test-to-predicted ratio of 0.945. Finally, Makino’s (1985) prediction provides conservative results with an average test-to-predicted ratio of 1.256.

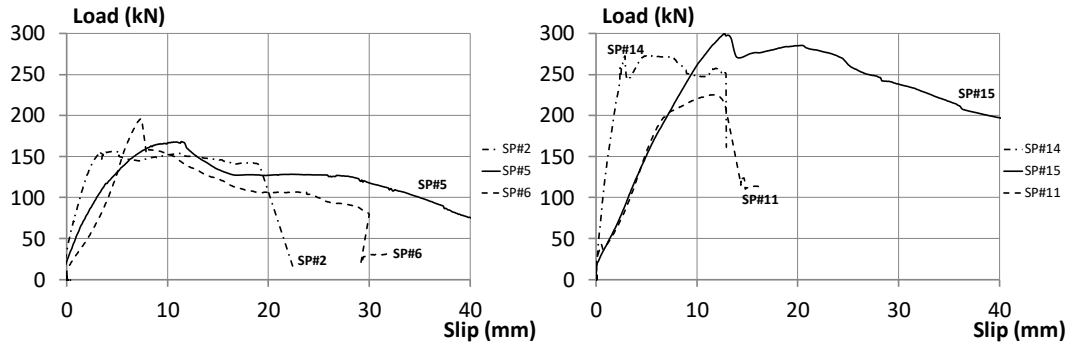


Specimen #18($h_{ef}/\phi=4.6$; $\phi=19\text{mm}$); Specimen #19($h_{ef}/\phi=4.6$; $\phi=19\text{mm}$); Specimen #23 ($h_{ef}/\phi=6.14$; $\phi=22\text{mm}$); Specimen #21($h_{ef}/\phi=7.37$; $\phi=19\text{mm}$)

Figure 13. Load-strain curves for SS configuration.

4.3. SINGLE ROW OF STUDS WITHOUT GROUP EFFECTS CONFIGURATION (SRS)

For this set of specimens, two studs are placed in a single row in the direction of loading. The distance between studs is larger than $3h_{ef}$ to avoid group effects according to the CCD approach proposed in ACI 318. Experimental results in the SRS configuration subjected to monotonic shear forces are shown in Table 4, and load-slip curves are plotted in Figure 14.



Specimen #2. ($h_{ef}/\phi=4.06$; $\phi=16\text{mm}$); Specimen #5. ($h_{ef}/\phi=4.6$; $\phi=19\text{mm}$); Specimen #6. ($h_{ef}/\phi=4.6$; $\phi=19\text{mm}$); Specimen #14. ($h_{ef}/\phi=6.28$; $\phi=22\text{mm}$); Specimen #15. ($h_{ef}/\phi=6.27$; $\phi=22\text{mm}$); Specimen #11. ($h_{ef}/\phi=7.26$; $\phi=19\text{mm}$)

Figure 14. Load-slip curve for SRS configuration.

Mixed concrete and steel failures were observed in Specimens #2, #5, #6 and #15. As shown in Figure 15, a concrete failure occurred, while the strains in the studs exceeded the yield strain (0.00175 m/m , see Figure 16). ACI 318 (Table 4) predicted similar results for concrete and steel failure for Specimens #2, #6 and #15, while Specimens #5 and #6 showed a half pyramid of concrete failure which may explain their low strength.

Table 3. Summary of experimental results for SS configuration.

					ACI 318 / AISC 360		EC-4		Makino	ACI 318		AISC 360	EC-4		Makino	
# SP	Ø (mm)	fc (MPa)	h _{ef} /Ø	Q _{test} (kN)	Concrete Strength Q _{cr} (kN)	Steel Strength AISC 360 Q _s (kN)	Concrete Strength Q _{cr} (kN)	Steel Strength Q _s (kN)	Strength Q (kN)	Q _{test} /Q _{cr}	Q _{test} /Q _s	Q _{test} /Q _s	Q _{test} /Q _{cr}	Q _{test} /Q _s	Q _{test} /Q _{cr}	Type of failure
18	19	24.5	4.68	97.71	104.75	127.59	72.15	102.07	71.43	0.933	0.766	0.766	1.354	0.957	1.368	Steel/Conc
19	19	41.4	4.63	120.31	133.37	127.59	111.06	102.07	100.46	0.902	0.943	0.943	1.083	1.179	1.198	Steel/Conc
23	22	37.5	6.14	157.86	164.76	171.06	137.87	136.84	126.29	0.958	0.923	0.923	1.145	1.154	1.250	Steel/Conc
21	19	41	7.37	120.74	173.93	127.59	110.23	102.07	99.82	0.694	0.946	0.946	1.095	1.183	1.210	Steel
							Avg (Max(Q _{test} /Q _{cr} , Q _{test} /Q _s))			0.945		0.894	1.217		1.256	
							Standard Deviation			0.010		0.086	0.092		0.077	

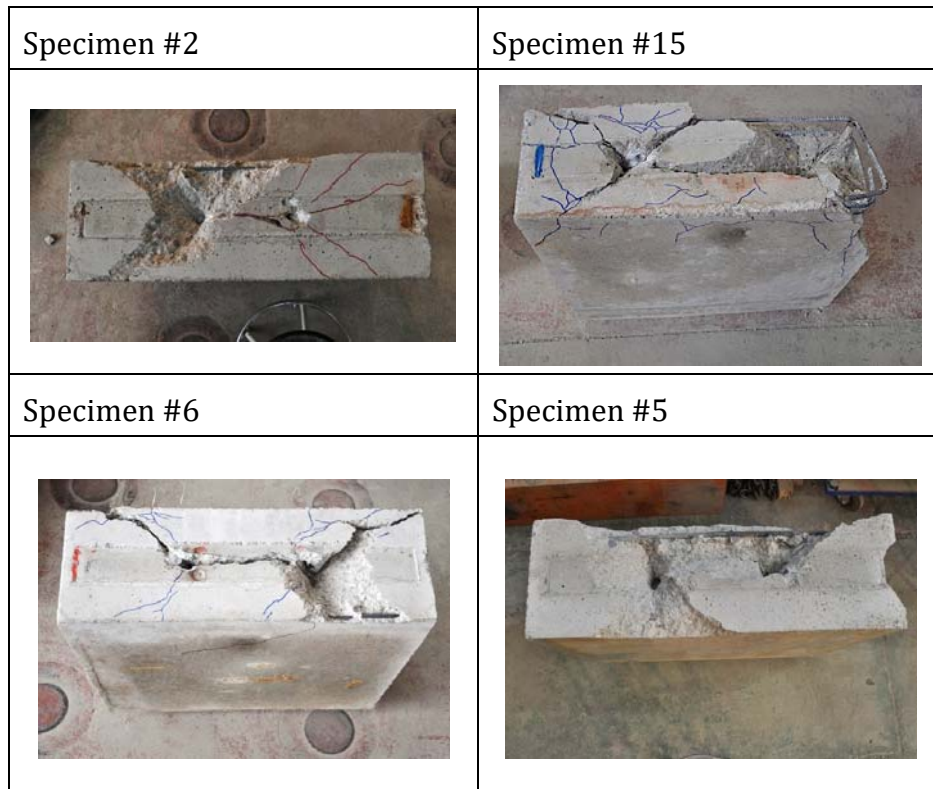
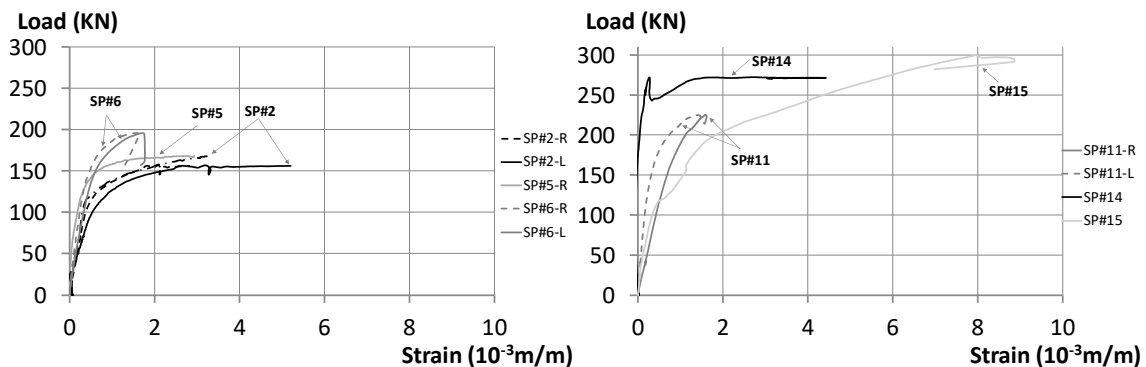


Figure 15. Mixed failures on tests for SRS configuration.

Specimen #11 showed a sudden drop in load after failure, while the remaining specimens sustained more moderate load losses after peak loads. Specimens #2 and #5 experienced a large strain in the studs, larger than 0.003 m/m. Additionally, specimen #6 reached the nominal yield strain (0.00175 m/m) of the stud, being the prediction of the steel strength by AISC 360 (255.2 kN) larger than the failure load of the test (196.1 kN). In this case, the EC-4 prediction of steel strength was relatively accurate (204.1 kN).



Specimen #2. ($h_{ef}/\phi=4.06$; $\phi=16\text{mm}$); Specimen #5. ($h_{ef}/\phi=4.6$; $\phi=19\text{mm}$); Specimen #6. ($h_{ef}/\phi=4.6$; $\phi=19\text{mm}$); Specimen #14. ($h_{ef}/\phi=6.28$; $\phi=22\text{mm}$); Specimen #15. ($h_{ef}/\phi=6.27$; $\phi=22\text{mm}$); Specimen #11. ($h_{ef}/\phi=7.26$; $\phi=19\text{mm}$)

Figure 16. Average of strains in the studs for Specimens #2, #5, #6, #11, #14 and #15.

Specimen #14 is also considered in the analysis despite the fact that the specimen failed in the weld (Figure 17) and Specimens # 9, #10 and #11 failed in the steel (Figure 18). The behavior of these specimens is similar to those with SS configuration since a) pyramidal failure surface in

concrete (Specimens #2 and #6), or the cracks defining this surface (Specimen #15), present a proper shape according to the CCD approach described in ACI 318; b) the pyramidal failure surface reaches the free edges of concrete and are restrained by the stirrups located on the upper side of the concrete; c) if failure occurs in the steel, a single plane of failure perpendicular to the stud axis is formed above the welded collar.



Figure 17. Welding failure in Specimen #14.

The average strength for this set of specimens is $0.850 f_u A_{sa}$ (Table 4), which means the strength is 15% lower than the steel failure predicted by ACI 318 or AISC 360. Taking into account a minimum of the steel and concrete strength predicted by EC-4, the strength estimation for this set was conservative as demonstrated by an average test-to-predicted ratio of 1.105. ACI 318 was not conservative for this set, with an average test-to-predicted ratio of 0.870. Makino's prediction was the most accurate with a mean test-to-predicted ratio of 1.067.



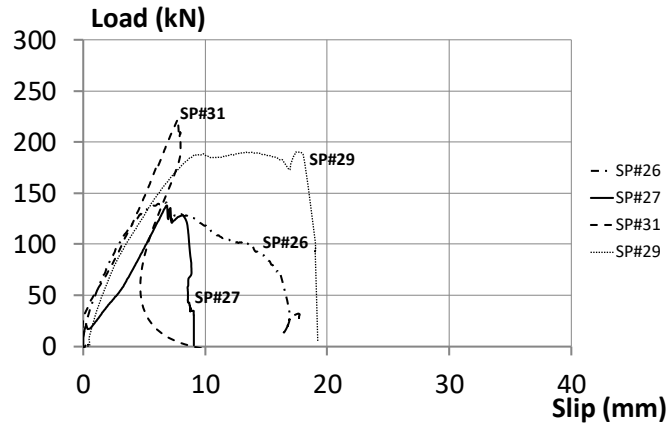
Figure 18. Steel failures on specimens for SRS configuration.

Table 4. Summary of experimental results for SRS configuration.

					ACI 318 / AISC 360		EC-4		MAKINO	ACI 318 / AISC 360		AISC 360	EC-4		MAKINO	
# SP	Ø (mm)	f _c (MPa)	h _{ef} /Ø	Q _{test} (kN)	Concrete Strength Q _{cr} (kN)	Steel Strength AISC 360 Q _s (kN)	Concrete Strength Q _{cr} (kN)	Steel Strength Q _s (kN)	Stud Strength	Q _{test} /Q _{cr}	Q _{test} /Q _s	Q _{test} /Q _s	Q _{test} /Q _{cr}	Q _{test} /Q _s	Q _{test} /Q _{cr}	Type of failure
2	16	48.4	4.06	156.69	183.08	180.96	177.34	144.77	157.7	0.856	0.866	0.866	0.884	1.082	0.994	Steel/Concrete
5	19	24.5	4.63	168.21	205.19	255.18	144.30	204.14	142.86	0.820	0.659	0.659	1.166	0.824	1.177	Steel/Concrete
6	19	41.4	4.61	196.07	264.47	255.18	222.11	204.14	200.91	0.741	0.768	0.768	0.883	0.960	0.976	Steel/Concrete
14	22	48.4	6.28	272.60	376.69	342.12	335.28	273.70	298.16	0.724	0.797	0.797	0.813	0.996	0.914	Weld*
15	22	41.4	6.27	300.01	348.22	342.12	297.79	273.70	269.37	0.862	0.877	0.877	1.007	1.096	1.114	Steel/Concrete
11	19	41.4	7.26	225.02	348.22	255.18	222.11	204.14	200.39	0.646	0.882	0.882	1.013	1.102	1.123	Steel
						Avg (Max(Q _{test} /Q _{cr} , Q _{test} /Q _s))				0.870	0.850	1.105	1.067			
						Standard Deviation				0.083	0.112	0.104	0.100			

4.4. TWO ROWS OF STUDS WITH GROUP EFFECTS CONFIGURATION (TRS-GE)

This configuration of specimens includes two studs placed next to each other in a direction orthogonal to the load (two rows). The distance between studs is less than $3h_{ef}$ and group effects are expected to appear based on the CCD approach in ACI 318. Experimental results in the TRS-GE configuration subjected to monotonic shear forces are shown in *Table 5*, and load-slip curves are plotted in *Figure 19*.



Specimen #26 ($h_{ef}/\phi=4.7$; $\phi=19\text{mm}$); Specimen #27 ($h_{ef}/\phi=4.5$; $\phi=19\text{mm}$); Specimen #31 ($h_{ef}/\phi=6.32$; $\phi=22\text{mm}$); Specimen #29 ($h_{ef}/\phi=7.37$; $\phi=19\text{mm}$)

Figure 19. Load-slip curve for TRS-GE configuration.

Concrete failure occurred in Specimens #26, #27 and #31. The slenderness ratios (h_{ef}/ϕ) for these specimens were between [4.5 – 6.5] and local failure of concrete limited the strength as compared to the single stud configuration. In the two rows of stud configuration, a small change was made in the model due to the presence of two close studs which increased the pyramid failure surface slightly and, as a consequence the predicted concrete resistance increased (between 2% and 9%). Steel strength of TRS-GE configuration, on the other hand, is double compared to the SS configuration. Also, in the TRS-GE configuration, concrete failures occurred for slenderness ratio h_{ef}/ϕ up to 6.5. Slenderness ratios larger than 6.5 presented steel failures in the TRS-GE configuration.

Specimen #26 (*Figure 20*) exhibited a proper pyramid surface failure around the studs according to CCD proposed in ACI 318. The experimental peak load was larger than the predicted load because the failure surface reached the upper stirrups of the concrete block which added resistance. Specimen #27 (*Figure 20*) presented an unexpected failure surface that resulted in an experimental load lower than predicted. Specimen #31 (*Figure 20*) had a larger failure surface and a brittle failure mode in the concrete. From the point of view of concrete strength predictions, specimens #26 and #31 revealed that the failure surface can be larger than the theoretical one and that these configurations reached a value 26% larger in terms of strength than that predicted by ACI 318.

The predictions made by the ACI 318 are conservatively closer to the test results (test-to-predicted ratio is 1.142) when group effects and trends to failure in concrete or mixed failure appear.

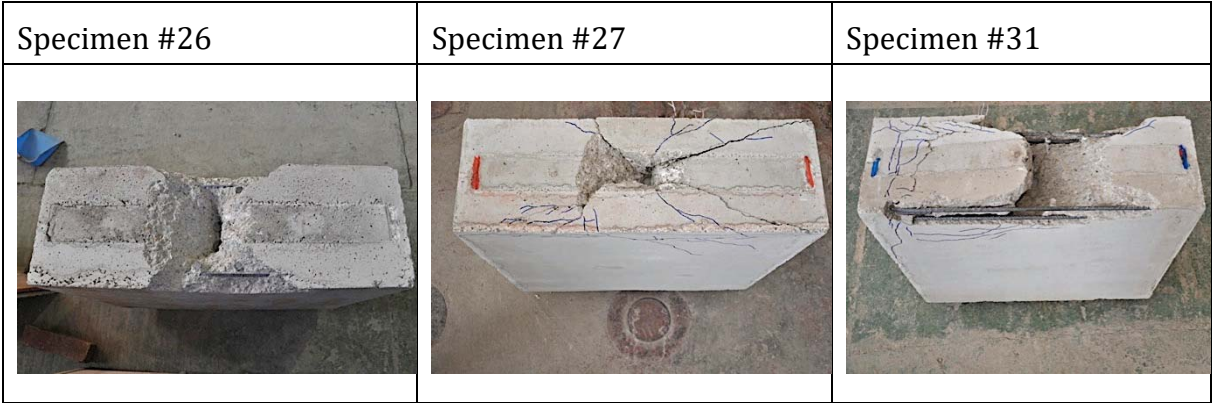
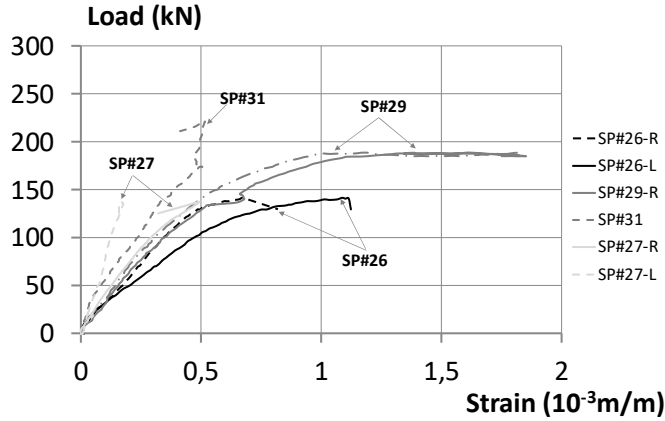


Figure 20. Concrete failure in TRS-GE configuration.



Specimen #26 ($h_{ef}/\phi=4.7$; $\phi=19\text{mm}$); Specimen #27 ($h_{ef}/\phi=4.5$; $\phi=19\text{mm}$); Specimen #31 ($h_{ef}/\phi=6.32$; $\phi=22\text{mm}$); Specimen #29 ($h_{ef}/\phi=7.37$; $\phi=19\text{mm}$)

Figure 21. Average of strains in the studs for specimens #26, #29 and #31.

Specimen #29 (Figure 22) presented a steel failure and was able to carry $0.746 A_s f_u$, which is a capacity 25% less than that predicted by ACI 318 and AISC 360. Again, the prediction by EC-4 fits the experimental data better (Q_{test}/Q_s by EC-4 is 0.932).

Similar to specimens #26 and #31, the strength of specimen #29 surpassed the predicted concrete strength, but in this case there were no notable cracks that would suggest a concrete failure. The larger slenderness ratio of specimen #29 ($h_{ef}/\phi = 7.37$) ensured a good embedment of the studs, although the group effects meant a weaker concrete limit state in the vicinity of the studs changing the failure mechanism from shear (without group effects) to tensile.

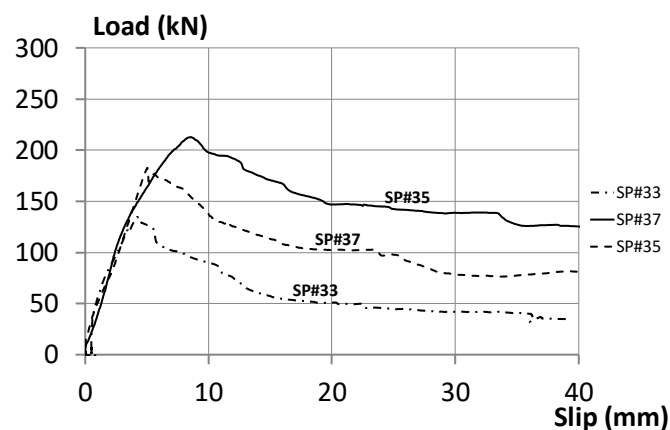
By contrast, Makino's (1985) predictions are the ones that best approximate (average of test-to-predicted is 0.964) the resistant behavior of headed studs in SFRCIW, since this author recommended these expressions for the proposed configuration of headed studs.



Figure 22. Steel failure in TRS-GE configuration.

4.5. SINGLE ROW OF STUDS WITH GROUP EFFECTS CONFIGURATION (SRS-GE)

In this configuration, two studs are located on the steel beam and separated by a distance less than $3h_{ef}$, such that group effects may reduce the strength. Experimental results in the SRS-GE configuration subjected to monotonic shear forces are shown in Table 6, and load-slip curves are plotted in Figure 23. All specimens were seen to have moderate drops in strength after the peak load indicating a degradation in the concrete around the studs.



Specimen #33 ($h_{ef}/\phi=4.5$; $\phi=19\text{mm}$); Specimen #35 ($h_{ef}/\phi=6.27$; $\phi=22\text{mm}$); Specimen #37 ($h_{ef}/\phi=7.11$; $\phi=19\text{mm}$)

Figure 23. Load-slip curve for SRS-GE configuration.

Concrete failure was observed in Specimen #33 with a slenderness ratio h_{ef}/ϕ between [4 – 4.5] while Specimens #35 and #37 with slenderness ratios between [5 – 7.5] presented mixed concrete and steel failures. In these two specimens, group effects and local concrete failure limited the resistance of the studs as demonstrated by the relatively modest increase in strength over the SS configuration, between 12% and 16%, while the area of the steel studs doubled. The increase in strength is associated with the slight increment in the size of the pyramidal failure surface.

Table 5. Summary of experimental results for TRS-GE configuration.

					ACI 318 / AISC 360		EC-4		MAKINO	ACI 318		AISC 360	EC-4		MAKINO	
#SP	Ø (mm)	f _c (MPa)	h _{ef} /Ø	Q _{test} (kN)	Concrete Strength Q _{cr} (kN)	Steel Strength AISC 360 Q _s (kN)	Concrete Strength Q _{cr} (kN)	Steel Strength Q _s (kN)	Stud Strength (kN)	Q _{test} /Q _{cr}	Q _{test} /Q _s	Q _{test} /Q _s	Q _{test} /Q _{cr}	Q _{test} /Q _s	Q _{test} /Q _s	Type of failure
26	19	24.5	4.71	141.38	115.75	255.18	144.30	204.14	127.78	1.221	0.554	0.554	0.980	0.693	1.106	Concrete
27	19	41.4	4.53	137.43	149.82	255.18	222.11	204.14	179.7	0.917	0.539	0.539	0.619	0.673	0.765	Concrete
31	22	41.4	6.34	222.41	170.70	342.12	297.79	273.70	240.93	1.303	0.650	0.650	0.747	0.813	0.923	Concrete
29	19	41	7.37	190.27	168.90	255.18	220.46	204.14	178.5	1.127	0.746	0.746	0.863	0.932	1.066	Steel
					Avg (Max(Q _{test} /Q _{cr} , Q _{test} /Q _s))					1.142	0.622	0.622	0.849	0.849	0.964	
					Standard Deviation					0.166	0.096	0.096	0.136	0.136	0.155	

Specimen #33 (Figure 24), exhibited a half pyramidal failure surface and premature concrete failure with a resulting ultimate load smaller than expected, similar to Specimens #23, #5 and #6, that did not develop full failure surface. In longer studs, such as Specimens #35 and # 37, the pyramidal failure surface is mostly developed around one of the studs, the one closest to the actuator, while the other stud failed in the steel (Figure 24). The concrete strength predicted by ACI 318 was reached.

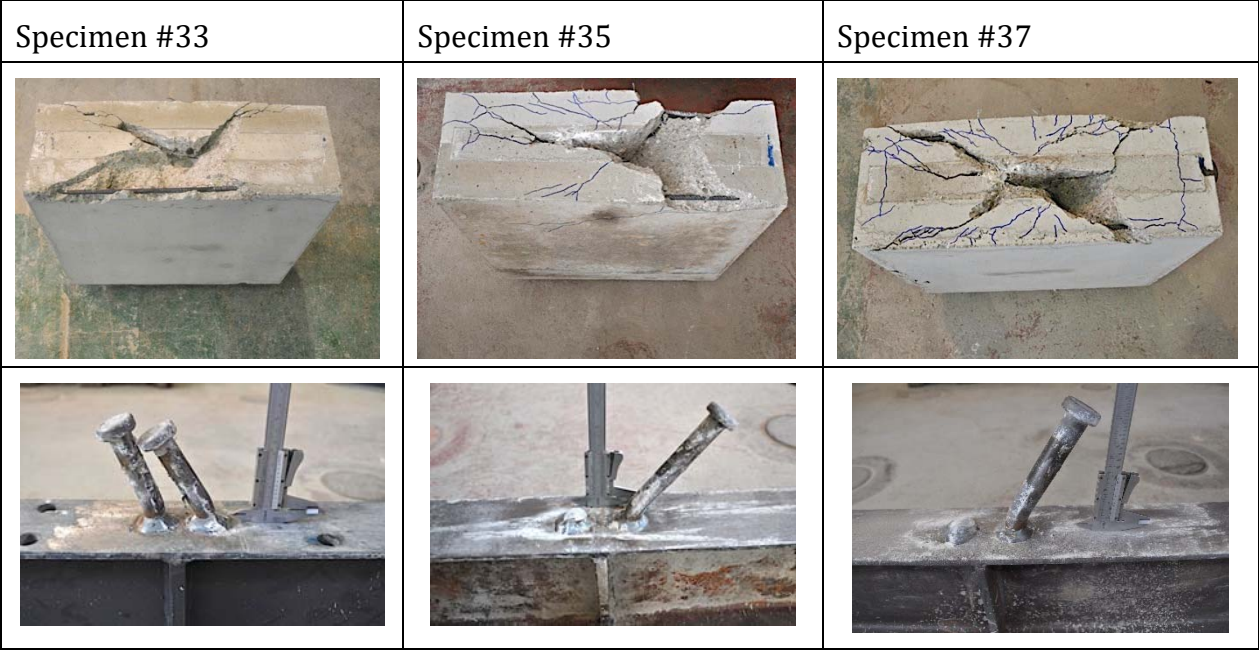


Figure 24. Concrete and mixed concrete and steel failure in SRS-GE configuration.

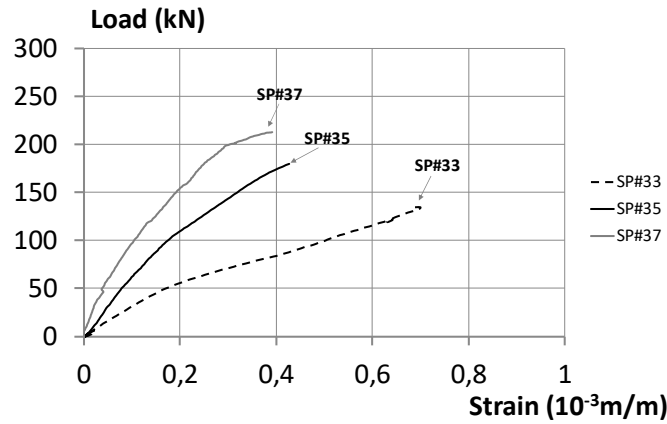
The behavior of this configuration of studs is similar to SS configuration since a) pyramidal failure reached the free edges of concrete and are restrained by the stirrups located on the upper side of the concrete; b) if failure occurred in the steel stud, a single plane of failure perpendicular to the stud axis was formed above the welded collar.

ACI 318 provisions were correct in detecting group effects in the prediction of local concrete failure. However, EC-4 and AISC 360 were not able to detect group effects (group effects are not considered in these specifications), resulting unsafe strength predications which is shown by test-to-predicted ratios of 0.777 and 0.621, respectively. Makino’s (1985) prediction also gave unsafe results as demonstrated by the test-to-predicted ratio of 0.821.

The strains registered in the stud were relatively small with values lower than 0.0007 m/m (Figure 25), which indicates that these studs were subjected to low values of tensile forces. Furthermore, it might be observed in Figure 25 that strains are smaller when the slenderness ratio is larger since it is better anchored for shear loading.

Table 6. Summary of experimental results for SRS-GE configuration.

# SP	Ø (mm)	f _c (MPa)	h _{ef} /Ø	Q _{test} (kN)	ACI 318 / AISC 360		EC-4		MAKINO	ACI 318 / AISC 360		AISC 360	EC-4		MAKINO	Type of failure		
					Concrete Strength Q _{cr} (kN)	Steel Strength AISC 360 Q _s (kN)	Concrete Strength Q _{cr} (kN)	Steel Strength Q _s (kN)	Stud strength (kN)	Q _{test} /Q _{cr}	Q _{test} /Q _s	Q _{test} /Q _s	Q _{test} /Q _{cr}	Q _{test} /Q _s	Q _{test} /Q _s			
33	19	37.5	4.50	134.45	142.41	255.18	205.67	204.14	188.4	0.944	0.527	0.527	0.654	0.659	0.714	Concrete		
37	22	37.5	6.27	212.58	191.72	342.12	275.74	273.70	252.5	1.109	0.621	0.621	0.771	0.777	0.841	Concrete		
35	19	41.4	7.05	182.97	200.29	255.18	222.11	204.14	200.9	0.914	0.717	0.717	0.824	0.896	0.911	Concrete		
					Avg (Max(Q _{test} /Q _{cr} , Q _{test} /Q _s))						0.989		0.622	0.777			0.821	
					Standard Deviation						0.105		0.095	0.118			0.099	



Specimen #33 ($h_{ef}/\phi=4.5$; $\phi=19\text{mm}$); Specimen #35 ($h_{ef}/\phi=6.27$; $\phi=22\text{mm}$); Specimen #37 ($h_{ef}/\phi=7.11$; $\phi=19\text{mm}$)

Figure 25. Average of strains in the studs for Specimens #33, #35 and #37.

4.6. SUMMARY OF RESULTS

From the experimental study, one may observe that steel and mixed concrete and steel failure modes are attained with stud slenderness ratios $h_{ef}/\phi > 4.5$ in configurations without group effects (SS and SRS) under monotonic shear loading. However, in configurations with group effects (TWS-GE and SRS-GE) subjected to shear loading with stud spacing between 42 and 65mm, the lower boundary slenderness to achieve steel failures is ($h_{ef}/\phi > 7$). A failure mode map for monotonic shear loading as a function of the stud configuration, stud spacing, and slenderness is given in Figure 26, taking into account experimental trends observed in tests.

		h/ϕ							
		4	4.5	5	5.5	6	6.5	7	7.5
		Mixed			Steel				
	$d > 3h_{ef}$	Concrete	Mixed		Steel				
	$42\text{mm} < d < 59\text{mm}$	Concrete			Mixed		Steel		
	$d = 64\text{mm}$	Concrete			Mixed		Steel		

Figure 26. Mapping failure modes in studs as a function of slenderness and configuration of studs under monotonic loading. (d : distance between studs).

According to Figure 27, when group effects are significant, only ACI 318 is formulated to capture the concrete strength at the studs in the presence of edge conditions. Steel Provisions (AISC 360 and EC-4) overestimate actual strengths provided by experimental results, being ACI

318 and Makino (for two rows of studs) the most accurate predictions. Neither EC-4 or Makino (1985) were as accurate at capturing group effects in anchors located in one row, with edge conditions of SFRCIW. Makino (1985) accurately predicted well the behavior of stud group effects located in two rows.

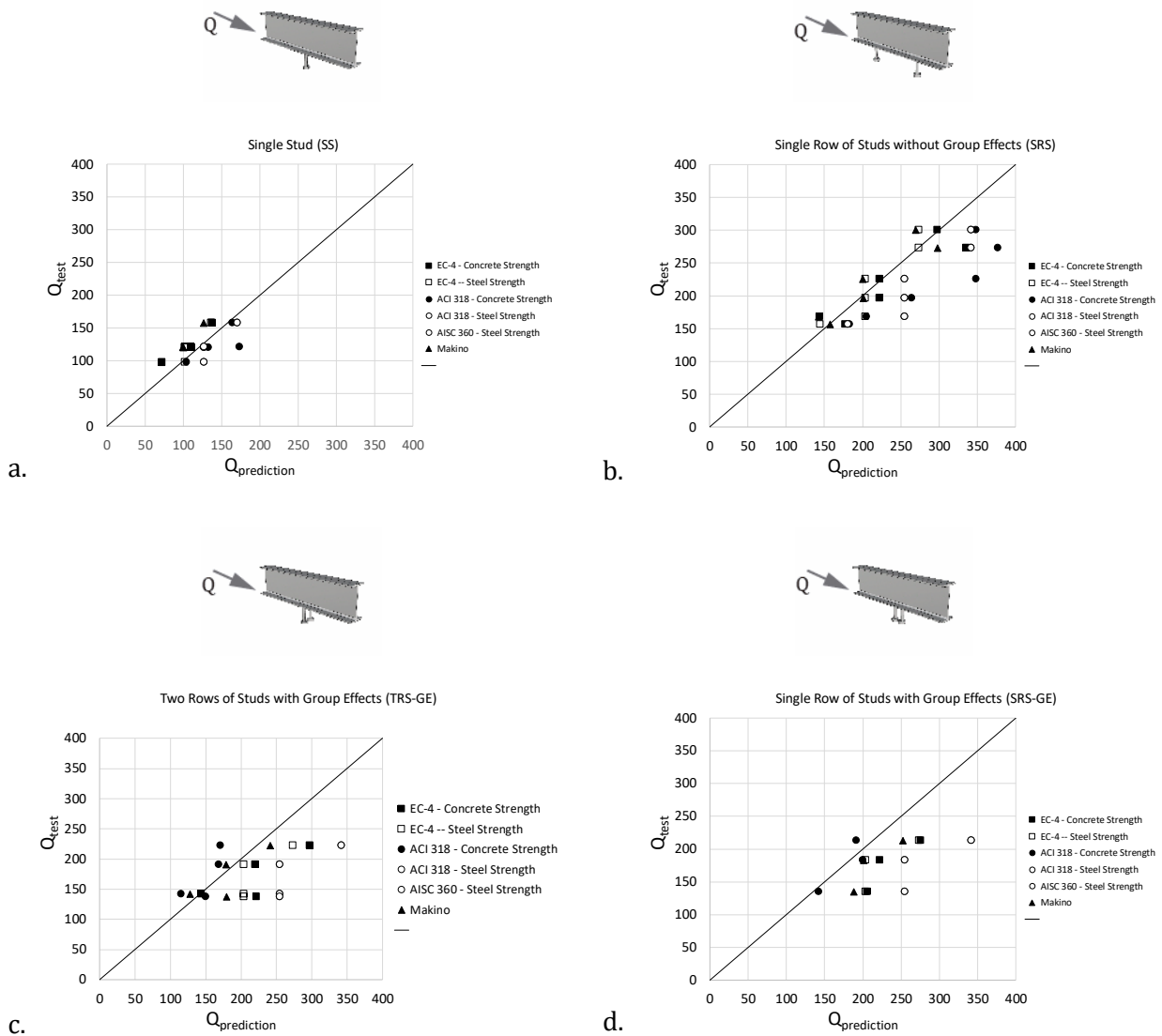
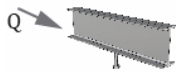
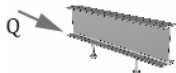
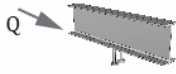
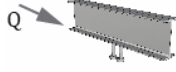


Figure 27. Summary of experimental and prediction comparisons for: a) SS configuration, b) SRS configuration, c) TRS-GE configuration and d) SRS-GE configuration.

The accuracy of stud strength predictions for SFRCIW using four methods is tabulated in Table 7. When group effects do not influence the behavior of the stud strength and the anchors present enough embedment in concrete to develop the full steel capacity, EC-4 ($0.8A_sF_u$) is generally conservative (10% to 20%) and ACI 318 and AISC 360 predictions for steel (F_uA_s) are somewhat less conservative (compared to $0.85A_sF_u$ observed strength). These predictions have an impact on the use of more conservative safety factors in the ACI 318 and the AISC 360.

Table 7. Monotonic predictions by ACI 318, AISC 360, EC-4 and Makino (1985).

$Q_{test}/Q_{predicted}$	ACI 318	AISC 360	EC-4	Makino (1985)
	0.870	0.850	1.105	1.067
	0.945	0.894	1.217	1.256
	1.142	-	0.849	0.964
	0.989	-	0.777	0.821

5. CONCLUSIONS

For this research a new test setup was designed to examine headed studs subjected to shear loading. The test setup simulates connections in SFRCIW and can capture edge conditions and group effects that might be typical of infill walls. An experimental design including 17 specimens was tested with monotonically applied shear force and the following conclusions may be drawn:

- The steel failure mode occurred for configurations of studs without group effects and a slenderness $h_{ef}/\varnothing > 4.5$ when subjected to shear loading.
- Configurations with group effects incorporating two studs subjected to shear loading with spacing between studs from 42mm to 65mm reached steel failure when slenderness ratios (h_{ef}/\varnothing) were larger than 6.2. Studs in SFRCIW might not develop the full steel strength in configurations with group effects (i.e. distances between studs smaller than $3h_{ef}$).
- An assessment of the ACI 318, AISC 360 and EC-4 provisions was made distinguishing cases with and without group effects. In the cases in which there are no group effects, the provisions provided good results with an average error of 10%. In the cases in which group effects of anchors are relevant, estimations by ACI 318 are relatively accurate, and EC-4 and Makino's formula produced non-conservative results (i.e. EC-4 average ratio for SRS-GE configuration Q_{test}/Q_{EC-4} of 0.777; EC-4 average ratio for TRS-GE configuration

Q_{test}/Q_{EC-4} of 0.849). When group effects were relevant in the design of studs installed in SFRCIW, ACI 318 was the only strength prediction that was able to capture group effects.

ACKNOWLEDGMENTS

The present study was funded by the Universitat Politècnica de València (UPV) and the Spanish Ministry of Economy and Competitiveness through the Project BIA2015-70651-R. The authors would like to express their gratitude to Debra Westall for revising the manuscript.

REFERENCES

1. ACI 318. *Building code requirements for structural concrete (ACI 318) and commentary (ACI 318R)*. Farmington Hills. Michigan. 2008.
2. AISC 360. *Load and Resistance Factor Design Specification for Structural Steel Buildings*. American Institute for Steel Construction. Chicago. Illinois. 2016.
3. AWS. *Structural welding code steel*. 2004.
4. Bursi, O. S. and Ballerini, M. "Behavior of a steel–concrete composite substructure with full and partial." *Proceedings of the Eleventh World Congress on Earthquake Engineering*. Acapulco: Elsevier. 1996. Paper 771.
5. Civjan, Scott A. and Prabhjeet Singh. "Behavior of shear studs subjected to fully reversed cyclic loading." *Edited by ASCE. Journal of Structural Engineering*. ASCE. 2003: 1466-1474.
6. Dall'Asta, A., Leoni, G., Morelli, F., Salvatore, W., and Zona, A. "An innovative seismic-resistant steel frame with reinforced concrete infill walls." *Engineering Structures*. Vol. 141. June 2017, Pages 144-158.
7. Eurocode 4. UNE - ENV 1994-1.1. *Design of composite steel and concrete structures. Part 1-1: General. Common rules and rules for buildings*. AENOR. 2004.
8. FEMA-461. *Interim Testing Protocols for Determining the Seismic Performance Characteristics of Structural and Nonstructural Components*. Redwood City. California. 2007.
9. Gattesco, N. and Giuriani, E. "Experimental study on stud shear connectors subjected to cyclic loading." *Journal of Constructional Steel Research* 38. no. 1 (1996): 1-21.
10. Hawkins, N.M. and Mitchell, D. "Seismic response of composite shear connections." *Journal of Structural Engineering (ASCE)* 110. no. 9 (1984): 1-10.
11. Klingner, R. E., Mendonca, J.A. and Malik J. B. "Effect of reinforcing details on the shear resistance of anchor bolts under reversed cyclic loading." *ACI Journal* 79. no. 1 (1982): 471-479.
12. Krawinkler, H., Gupta, A., Medina, R. and Luco, N. *Development of Loading Histories for Testinf of Steel Beam-to-Column Assemblies*. Stanford University. Stanford. 2000.

13. Lindquist, M. R. "Final report USNRC anchor bolt study: Data survey and dynamic testing." *U.S. Nuclear Regulatory Commission. NUREG/CR-2999*. 1982.
14. Makino, M. "Design of framed steel structures with infill reinforced concrete walls." Edited by Roeder CW. ASCE. New York: ASCE. 1985. 279-87.
15. Morelli, F., Mussini, N., and Salvatore, W. "Influence of shear studs distribution on the mechanical behaviour of dissipative hybrid steel frames with r.c. infill walls." *Bulletin of Earthquake Engineering*. Vol. 17, Issue 2, 2019, Pages 957-983.
16. Morelli, F., Caprili, S. and Salvatore, W. "Dataset on the cyclic experimental behavior of Steel frames with Reinforced Concrete infill Walls." *Data in Brief Open Access*. Vol. 19, August 2018, Pages 2061-2070.
17. Pallarés, L. and Hajjar, J.F., "Headed Steel Stud Anchors in Composite Structures: Part I. Shear." *Report No. NSEL-013. Newmark Structural Laboratory Report Series (ISSN 1940-9826)*. 2009.
18. Pallarés, L. and Hajjar, J. F. "Headed steel stud anchors in composite structures. Part I: Shear." *Journal of Constructional Steel Research (Elsevier)* 66. no. 2 (2010): 198-212.
19. Pavlovic, M., Markovic, Z., Veljkovic, M. and Budevac, D. "Bolted shear connector vs. headed studs behavior in push-out tests." *Journal of Constructional Steel Research* 88 (2013): 134-149.
20. Saari, W. K., Hajjar, J.F., Schultz, A.E. and Shield, C.K. "Behavior of shear studs in steel frames with reinforced concrete infill walls." *Journal of Constructional Steel Research*. 2004: 1453-1480.
21. Zandonini. R. and Bursi, O.S. "Cyclic behavior of headed shear stud connectors." Edited by J F Hajjar. M Hosain. W S Easterling and B M Shahrooz . *Composite construction in steel and concrete IV*. Reston: ASCE. 2002. 470-82.